Available online at www.sciencedirect.com
SCIENCE DIRECT®
Acta Materialia 53 (2005) 3369–3382
Acta MATERIALIA
www.actamat-journals.com

Mechanistic models for the activation volume and rate sensitivity in metals with nanocrystalline grains and nano-scale twins

Robert J. Asaro [a], Subra Suresh [b,*]

[a] Department of Structural Engineering, University of California, San Diego La Jolla, CA 92093, United States
[b] Department of Materials Science and Engineering, Massachusetts Institute of Technology, 77 Massachusetts Avenue, Cambridge, MA 02139-4307, United States

Received 23 November 2004; received in revised form 28 March 2005; accepted 28 March 2005
Available online 23 May 2005

Abstract

This paper describes mechanistic models that seek to rationalize experimentally determined low values for the activation volume associated with the high strain rate sensitivity of nanocrystalline metals. We present models for the emission of partial or perfect dislocations from stress concentrations at a grain boundary or twin boundary. The emission of deformation twins is likewise examined as a competing mechanism to perfect dislocation emission. The approach illustrates the important roles of both the intrinsic stacking fault energy and the unstable stacking energy. We find that the models lead to estimates of activation volumes in the range $3 - 10b^3$ for truly nanocrystalline metals. Activation volumes are found to increase monotonically with increasing grain size. The findings are found to be in accord with available experimental evidence in both a quantitative and qualitative manner. Deficiencies in the available experimental evidence are noted, specifically in the context of explaining some of the difficulties in comparing theoretical predictions to experimental observation.

Keywords: Nanostructured metals; Twinning; Strain rate sensitivity; Mechanical properties; Modeling

1. Introduction and overview

It has been recognized for several decades that metals and alloys with grain dimensions smaller than 100 nm (so-called nanostructured or nanocrystalline metals and alloys) generally exhibit substantially higher strength than their microcrystalline counterparts with grain dimensions typically larger than, say, 1 μm (e.g. [1–4]). Moreover, there is mounting experimental evidence from recent investigations which point to the following additional mechanical characteristics of nanostructured metals.

- The plastic deformation characteristics of nanocrystalline face-centered-cubic (fcc) metals are much more sensitive to the rate of loading than those of microcrystalline fcc metals. The strain-rate sensitivity index, defined below, is an order of magnitude higher for metals with nanocrystalline structures [5–11].
- The activation volume, which is broadly defined as the rate of decrease of activation enthalpy with respect to flow stress at fixed temperature and which influences the rate-controlling mechanisms in the plastic deformation of engineering metals and alloys, is some two orders of magnitude smaller for nanocrystalline metals than for microcrystalline metals [10,11].
- The abundance of grain boundaries providing obstacles to dislocation motion during plastic deformation generally leads to enhanced strength in nanocrystalline

* Corresponding author. Tel.: +1 617 253 3320; fax: +1 617 253 0868.
E-mail address: ssuresh@mit.edu (S. Suresh).

1359-6454/$30.00
doi:10.1016/j.actamat.2005.03.047

metals. However, twin boundaries (which are special kinds of coherent internal interfaces) are also known to obstruct dislocation motion. Recent experiments show that the introduction of nano-scale twins within ultrafine crystalline metals, with average and range of grain size within the 100 nm to 1 μm regime, leads to significant increases in flow stress and hardness [11,12]. The extent of such strengthening is comparable to that achievable by nanocrystalline grain refinement.[1]

- The incorporation of nano-scale twins during the processing of metals with ultrafine grains is also known to increase the loading rate sensitivity by almost an order of magnitude and decrease the activation volume by two orders of magnitude as compared to the values observed in microcrystalline metals [11].

Thermally activated mechanisms contributing to plastic deformation processes in metals and alloys are often quantitatively interpreted by examining the rate sensitivity index, m, and activation volume, υ. The non-dimensional strain-rate sensitivity index is defined as [13,9]

$$m = \frac{\sqrt{3}kT}{\upsilon\sigma} = \frac{3\sqrt{3}kT}{\upsilon H}, \tag{1}$$

where k is the Boltzmann constant, T the absolute temperature, σ the uniaxial flow stress, H the hardness (which is generally assumed to be three times the flow stress), and

$$\upsilon = \sqrt{3}kT\left(\frac{\partial \ln \dot{\epsilon}}{\partial \sigma}\right), \tag{2}$$

where $\dot{\epsilon}$ is the strain rate as measured in uniaxial tension for instance. (See, for instance, Krausz and Eyring [14] for a general discussion of thermally activated rate theory as applied to deformation kinetics.)

The implications of grain refinement on strengthening and hardening in fcc metals is summarized in Figs. 1 and 2 for Cu and Ni, respectively. Available data (see, for example [11,12,15–22]) showing the dependence of flow stress on grain size, over the nm to the μm range, for polycrystalline Cu are plotted in Fig. 1. Here the flow stress varies more or less linearly with $d^{-1/2}$ where d is the grain size. The red star symbols in Fig. 1 pertain to ultrafine-grained Cu with growth twins where the twin width l is plotted in place of the grain size. Note that the twin width exhibits the same connection to flow stress as the grain size in nano-twinned Cu.

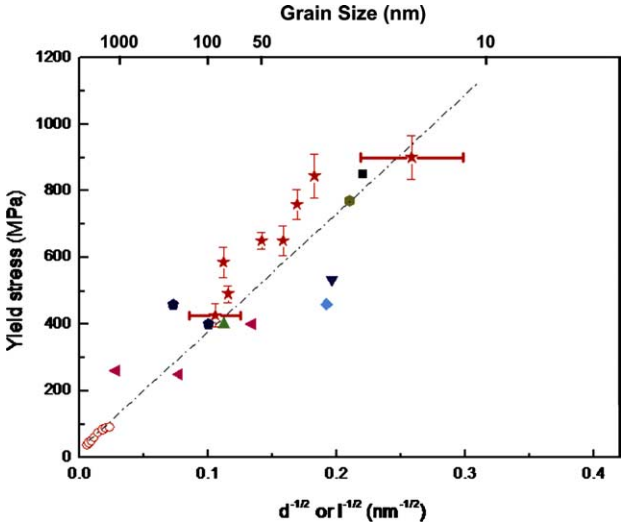

Fig. 1. A plot of the yield stress as a function of inverse square root grain size from experimental data obtained on nano-, ultrafine- and micro-crystalline pure Cu. Also indicated in the figure are data (denoted by red star symbols with scatter range) for Cu with controlled growth twins for which the twin width l is plotted in place of the grain size d. The different color symbols denote data from different sources [11,12,15–22].

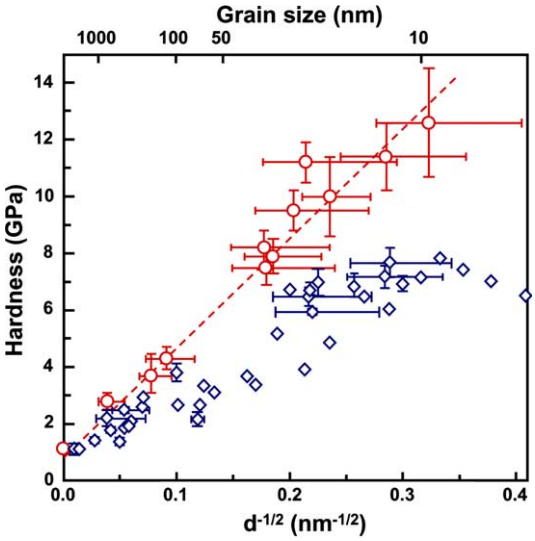

Fig. 2. Variation of hardness as a function of grain size (top abscissa axis) or inverse square root grain size (bottom abscissa axis) for polycrystalline Ni with grain size from nano-, ultrafine- and micro-crystalline regimes from several investigators [7–9,17,23–28], indicated by the blue-colored data points. The red points with scatter ranges denote data extracted from instrumented nanoindentation experiments on thin Ni foils produced by pulsed laser deposition on different hard substrates [34].

Fig. 2 is a plot of indentation hardness versus decreasing grain size for polycrystalline Ni spanning

[1] Strengthening of metals and alloys by recourse to grain refinement in the nano-scale also increases the scattering of conducting electrons at the grain boundaries. This leads to a deterioration of electrical conductivity. On the other hand, the introduction of coherent twins with nano-scale dimensions inside much larger grains can offer the same level of strengthening as nanocrystalline grains [11,12]. In addition, it circumvents the potential drawbacks inherent in grain refinement because the electrical resistivity of coherent twin boundaries is an order of magnitude smaller than that of high-angle boundaries [12].

the nanostructured to the microstructured grain dimensions. The data points indicated in blue denote experimental results obtained on nanocrystalline and ultrafine crystalline Ni produced by such techniques as electrodeposition, powder consolidation and inert gas condensation followed by compaction [7–9,17,23–28]. These results indicate that the hardness of Ni departs significantly from the classical Hall–Petch type behavior when the grain size is reduced typically below about 100 nm. In addition, a lowering of hardness with grain refinement has been reported [26] for Ni below a grain size of approximately 8 nm. Such a transition from strengthening to weakening with grain refinement has been postulated from computational simulations [4,29–31] and by invoking concepts of grain boundary sliding associated with room temperature creep [32]. Experimental simulations of indentation of two-dimensional nanocrystalline structures employing the polycrystalline bubble raft analogues also revealed a transition from primarily dislocation nucleation at grain boundary triple junctions to a greater propensity for grain boundary sliding when the average grain size of the crystals in the draft was reduced below about 7 nm [33]. By contrast, hardness values (indicated by the red data points in Fig. 2 extracted from instrumented nanoindentation for nanocrystalline Ni foils pulse-laser-deposited on different hard substrates [34]) appear to show a different trend. Here, one observes strengthening with grain refinement down to about 10 nm or so in a manner consistent with the expectations predicated upon the classical Hall–Petch behavior. It is evident from the results displayed in Fig. 2 that despite the growing body of experimental results on the deformation characteristics of nanostructured metals, considerable uncertainty exists about the mechanisms responsible for deformation, especially at very small grain sizes.

Fig. 3 provides a summary of the experimental results available to date in the literature on the variation of m as a function of grain size for micro-, ultrafine-, and nanocrystalline metals and alloys. It is evident here that a reduction in grain size from the micro- to the nanocrystalline regime causes an order of magnitude increase in the strain rate sensitivity of plastic deformation. Results are shown for Cu with a fixed grain size of 500 nm which was pulse-electrodeposited in such a way that the grains contained nano-scale twins with widths of approximately 20 or 90 nm. The twin width is indicated in Fig. 3 for these cases in place of the grain size. Available data indeed indicates a trend of increased rate sensitivity at higher strain rates, as also shown in [10] for ultrafine grained Cu a grain size of approximately 300 nm.

A summary of available data [5,8–11,28,35–41] on the effect of grain size on the activation volume of Cu and Ni is shown in Fig. 4. Note the decrease in activation volume with grain refinement. The activation volume

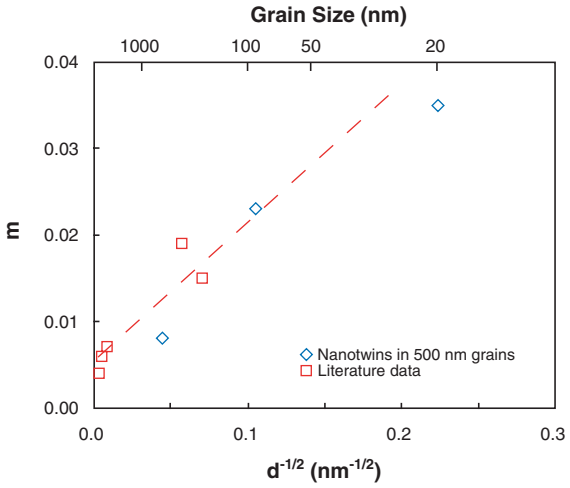

Fig. 3. A plot of the effect of grain size on the loading rate sensitivity index, m, of pure Cu and Ni at room temperature from available literature data [8,9,11,28,35–41]. Also indicated are points taken from [11], denoted by open diamonds, for pure Cu where twins with a width of 20 or 90 nm were introduced by pulsed electrodeposition inside grains with an average size of approximately 500 nm. For these cases, the twin width is plotted instead of the grain size.

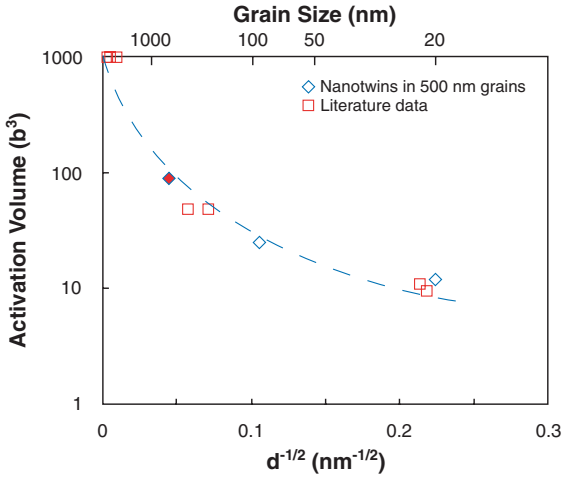

Fig. 4. A plot of the effect of grain size on the activation volume, measured in units of b^3, for pure Cu and Ni from available information [5,8–10,28,35–41]. Also indicated are two data points, denoted by open diamonds (corresponding to the same set of experiments for which m values were shown in Fig. 3), for pure Cu where twins with a width of 20 or 90 nm were introduced via pulsed electrodeposition inside grains with an average size of 500 nm (from [11]). For these cases, the twin width is plotted instead of the grain size.

for the ultrafine-grained Cu specimens with nano-twins [11] is also indicated in this figure, with the twin width replacing the grain size as the characteristic structural length scale. Note the 100-fold increase in activation volume as the spacing of the internal interface is varied from about 20 to about 100 nm.

The foregoing observations clearly illustrate the effects of nanocrystalline grains and nano-scale twins on

strength, hardness, rate sensitivity of deformation and activation volume. However, the mechanisms underlying such trends are not well understood at the present time. In addition, quantitative, analytical formulations are not available for rationalizing the observed variations in parameters as the characteristic structural length scales are altered by several orders of magnitude. It was, indeed, these limitations in current understanding that motivated the present study.

The overall objective of the present work was to develop mechanism-based models that rationalize the distinct deformation characteristics of fcc metals with grain size and twin dimensions in the nanometer regime. This paper develops estimates of flow stress as a function of strain rate and activation volume by exploring the roles of crystal stacking energies, such as the *intrinsic stacking fault* and the *unstable stacking energy*, in the process of initiating deformation via the emission of either partial dislocations, i.e., stacking faults, or perfect dislocations from the grain or twin boundaries of nanostructured fcc metals. This goal is accomplished through the exploration of two mechanistic processes: (i) a pre-existing boundary dislocation emits a segment of a partial or perfect dislocation into the grain, or (ii) the spontaneous emission of a partial or perfect dislocation from a source of stress concentration at the boundary. The latter process is envisioned as arising from a scenario where a crack-like stress concentrator such as a freely slipping grain boundary facet begins to slide and concentrates stress with a near $1/\sqrt{r}$ type singular field ahead of it. The predictions of these models are correlated with available experimental data and with the phenomenology extracted from molecular dynamics simulations.

The plan of the paper is as follows. The next section begins with a brief review of a model due to Asaro et al. [42] that deals with the emission of a partial dislocation into a nano-scale grain. The model is extended here to describe the emission of a trailing partial, or a second leading partial on an adjacent slip plane to form a deformation twin so as to rationalize the significance of the intrinsic stacking fault energy in controlling strength. Following that, we describe a model for the emission of a leading partial dislocation and then its trailing partial dislocation from a stress concentrator at a grain boundary facet. This analysis shows that aside from the stacking fault energy alone, the *unstable stacking energy*, introduced by Rice [45], plays an important role in determining the critical condition for the emission of a partial as well as a full dislocation. Its meaning is discussed below in Section 3.1. Deformation twins are treated in a similar manner in a later section. A model for the nucleation of a partial dislocation at a stress concentration is then described. We note that our modeling of the nucleation process is motivated inter alia by direct observation of dislocation nucleation at boundaries including growth twin boundaries as seen in the recent work of Lu et al. [11] (discussed further in later discussion). It is shown that the results emerging from the present analysis directly lead to estimates of the range of values for activation volume and rationalize the empirical trends regarding the observed high strain- and loading-rate sensitivity described above. This is followed by related discussion and conclusions.

2. Emission of partial and perfect dislocations from existing grain boundary dislocations

Our analysis begins with consideration of a partial, or perfect, dislocation emitted from a grain boundary, as envisioned in [42] and schematically sketched in Fig. 5. To set the geometry, let the perfect dislocation have a Burgers vector along the unit crystal axis **s**, and let the unit normal to the slip plane of the perfect dislocation be **m**; **z** is the third unit vector of the (**s**, **m**, **z**) triad. Then the criterion for emission of a segment of partial dislocation into the grain, of diameter d, and for extending it entirely through the grain, is [42]

$$\left\{\frac{\tau_{ms}}{G}\frac{b_s^{(1)}}{|b|}+\frac{\tau_{mz}}{G}\frac{b_z^{(1)}}{|b|}\right\}=\frac{(\alpha-1)}{\alpha}\Gamma+\frac{1}{3}\frac{b}{\bar{d}}. \tag{3}$$

Here the dislocation is taken to be composed of the lead partial, $\mathbf{b}^{(1)}$, and a trailing partial, $\mathbf{b}^{(2)}$; the full Burgers vector is $\mathbf{b}=\mathbf{b}^{(1)}+\mathbf{b}^{(2)}$. The components of such partial dislocations, all of which lie in the slip plane of the parent dislocation, are $\mathbf{b}_s^{(1)},\mathbf{b}_z^{(1)},\mathbf{b}_s^{(2)}$ and $\mathbf{b}_z^{(2)}$. The shear stress components that are work conjugate to these partial components are τ_{ms} and τ_{mz}. Also, b is the magnitude of the perfect dislocation's Burgers vector, $\bar{d}$ the grain size, $\alpha=\bar{d}/\delta_{\mathrm{eq}}$, where δ_{eq} is the equilibrium spac-

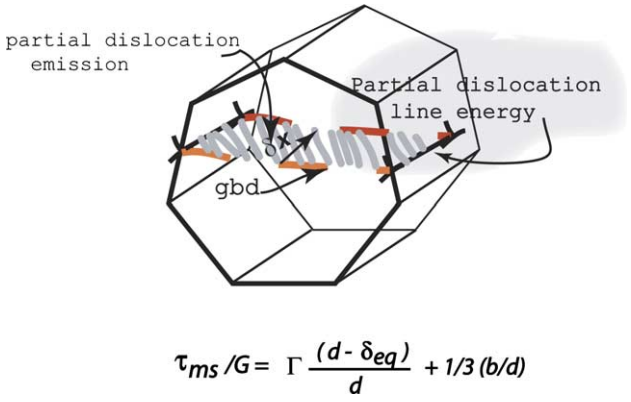

Fig. 5. A composite model for SF emission from a grain boundary. The model assumes the existence of a dislocation in a grain boundary, a partial or perfect segment which is emitted into the grain. Note that segments of dislocation are created on the side boundaries of the grain and their energy must be accounted for as well as the energy of the faults that are created by the emission of partial dislocations. Note that the line energy of a partial dislocation segment in an fcc metal is taken as $1/2(1/3)Gb^2$ since the magnitude of the Burgers vector is $1/\sqrt{3}b$.

Table 1
Sample values of critical resolved shear stress, along the direction of the Burgers vector of the perfect dislocation, to emit a partial dislocation from a preexisting grain boundary dislocation

$\bar{d}$ (nm)	50	30	20	10	δ_{eq}	$\Gamma/(Gb)$
Cu	211 MPa	248 MPa	291 MPa	421 MPa	1.6 nm	1/250
Ni	960 MPa	1027 MPa	1115 MPa	1381 MPa	0.5 nm	1/100
Ag	125 MPa	158 MPa	198 MPa	321 MPa	3.4 nm	1/447
Pd	719 MPa	763 MPa	820 MPa	988 MPa	0.54 nm	1/75

ing of partial dislocations in the unstressed crystal, and G is the shear modulus. The *reduced stacking fault energy* is $\Gamma = \gamma_{sf}/Gb$ where γ_{sf} is the intrinsic stacking fault energy. In terms of it, the equilibrium spacing of partial dislocations, δ_{eq}, in an unstressed crystal is

$$\delta_{eq} \approx \frac{1}{12\pi}\frac{b}{\Gamma}. \tag{4}$$

Before examining the consequences of this model for estimating the strength of nanostructured crystals, we will explore a second possible mechanism for emitting partial dislocations. For now, however, we list in Table 1 some sample estimates for several fcc metals, derived from Eq. (3), for critical resolved shear stresses to drive lead partial dislocations into a nanostructured grain, i.e., resolved along the direction of the lead partial dislocation.

For later reference, and as an example, note that for Ni with a grain size of 20 nm the critical stress is on the order of 1100 MPa whereas later discussion will show that the alternative model we explore leads to even larger values. Also later, we use these estimates to approximate what would be expected to be the uniaxial tensile flow stress by using the connection, $\sigma \approx 2 \times \tau$, where τ is the estimated resolved shear stress. It should be noted for later reference that this model is three-dimensional in the sense that it specifically considers the formation of segments of dislocation in the side boundaries of the grain as shown in Fig. 5. As observed below, these segments contribute to the energy required to emit the dislocation and consequently contribute to the flow stress required to drive deformation.

This model also provides a compelling picture of the role of stacking fault energy in controlling strength. Transitions to other mechanisms, in particular grain boundary sliding and the emission of perfect dislocations, can also be examined by extending this approach. For example, if τ is the shear stress resolved along the direction of the lead partial dislocation, then the relation in Eq. (3) can be simplified as

$$\frac{\tau}{G} = \frac{(\alpha-1)}{\alpha}\Gamma + \frac{1}{3}\frac{b}{\bar{d}}. \tag{5}$$

A perfect dislocation can be emitted [42] when

$$\frac{\tau}{G} = \frac{b}{\bar{d}}, \tag{6}$$

and, therefore, a transition from full to partial dislocation is expected at a grain size, $\bar{d}_t$, where

$$\frac{b}{\bar{d}_t} = \frac{3}{2}\frac{(\alpha-1)}{\alpha}\Gamma \Rightarrow \bar{d}_t = \frac{2}{3}\frac{\alpha}{\alpha-1}\frac{b}{\Gamma}. \tag{7}$$

Note that this type of model introduces a grain size dependence via the geometry of the "side segments" as depicted in Fig. 5. Using the values for the reduced stacking fault energy found in Table 1, and approximating $\alpha/(\alpha-1) \approx 1$, values for $\bar{d}_t$ are found[2] as listed in Table 2.

The picture that emerges from the values in Table 2 is that for metals such as Ni and Pd, it is more likely that deformation involves perfect dislocations or at least partial and trailing dislocations rather than lead partial dislocations and stacking faults only. This is particularly true for nanocrystals with grain sizes $\bar{d} \geqslant 15$ nm or so. For metals such as Cu, and more especially Ag with a relatively low stacking fault energy, faults are more likely to be observed as the result of partial dislocation emission only. Metals such as Al, with a relatively high stacking fault energy, would likewise be expected to emit perfect dislocations rather than intrinsic stacking faults. We consider later the possibility of deformation twins being emitted and estimate relative trends for twin nucleation as opposed to dislocation or fault emission. Experimental observations are clearly required to document the actual trends. The trends identified here appear to be quite consistent with the results of recent molecular dynamics simulations [43] for nanostructured Ni, Al, and Cu. These simulations reveal that in Al, perfect dislocations tend to be emitted, whereas in Cu partial dislocations are emitted at triple points, and in Ni extended partial dislocations are seen to traverse entire grains. Furthermore, in Al, perfect dislocations are emitted by the initiation of a leading partial followed closely by its trailing counterpart as would be forecast by the modeling presented herein.

The condition for partial dislocation emission described by Eq. (3) is for the extension of a partial entirely across a grain. The discussion surrounding the analysis of partial emission from a stress concentrator such as

[2] This approximation must be taken with care for metals such as Ag that has a rather low intrinsic stacking fault energy. For grain sizes below 10 nm the factor $(\alpha-1)/\alpha$ falls measurably below unity.

Table 2
Values for the Burgers vector and $\bar{d}_t$

	Cu	Ni	Ag	Pd
b (nm)	0.255	0.248	0.288	0.275
$\bar{d}_t$ (nm)	40	16	84	13

a grain boundary facet or triple point to be considered in the next section makes clear, however, that both leading and trailing partial dislocations will be emitted with spacings that depend on both the unstable stacking energy and the stacking fault energy. This more general scenario is depicted in Fig. 6. The foregoing analysis of the degree of extension of partial dislocations and the model from [42] readily provide the energy of the system depicted in Fig. 6 and it contains the terms

$$\mathscr{E} = -2\mathscr{K}_{ij}b_i^{(1)}b_j^{(2)}\ln(\delta/r_0) - (\tau_{ms}b_s^{(1)} + \tau_{mz}b_z^{(1)})(\delta + s - r_0)\bar{d} - (\tau_{ms}b_s^{(2)} + \tau_{mz}b_z^{(2)})(s - r_0)\bar{d} + 2\mathscr{L}_{\mathrm{p}}\delta + 2\mathscr{L}_{\mathrm{f}}s + \gamma_{\mathrm{sf}}\delta\bar{d}. \tag{8}$$

Here $\mathscr{L}_{\mathrm{p}}$ and $\mathscr{L}_{\mathrm{f}}$ are the energies per unit length of a partial and full dislocation, respectively. $\mathscr{K}$ is the *energy factor matrix* defined by Barnett and Asaro [44], and for an elastically isotropic material with the dislocation lying along the **s** direction for example, $\mathscr{K}_{mm} = \mathscr{K}_{zz} = G/4\pi(1-\nu)$, and $\mathscr{K}_{ss} = G/4\pi$. For brevity, let $\tau_1 = \tau_{ms}b_s^{(1)} + \tau_{mz}b_z^{(1)}$ and $\tau_2 = \tau_{ms}b_s^{(2)} + \tau_{mz}b_z^{(2)}$. γ_{sf} is, again, the intrinsic stacking fault energy. When $\mathscr{E}$ is minimized with respect to δ, the extension of the partial dislocations, it is seen that

$$\delta_{\mathrm{eq}} = \frac{2\mathscr{K}_{ij}b_i^{(1)}b_j^{(2)}}{\gamma_{\mathrm{sf}} - \tau_1 + 1/3\left[Gb^2/\bar{d}\right]}. \tag{9}$$

The factor of 1/3 in the term in the denominator arises from the ratio of magnitude of the Burgers vector of the partial to that of a perfect dislocation. This result shows, inter alia, that under stress, partial dislocations may extend considerably further than when the system is unloaded and δ_{eq} is as given in Eq. (4). Now when $\mathscr{E}$ is minimized with respect to s, what follows is a criterion independent of s, and we recover the original criterion [42] for emitting a full dislocation, viz., the relation given above in Eq. (6), since the resolved shear stress, τ, used in Eq. (6) is in fact the same as $\tau_1 + \tau_2$.

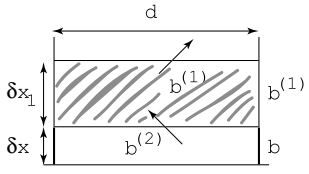

Fig. 6. Emission of a leading partial dislocation followed by its trailing partial dislocation. The spacing between the two partial dislocations depends on the two stacking energies as described in the text. In some cases, i.e., in materials with low stacking fault energy, the leading partial dislocation will spread entirely across the grain, whereas in materials with high, or moderately high stacking energies, either full dislocations or complexes containing very large faults will be observed.

3. Emission of a partial dislocation from a stress concentration

A second possible mechanism, alluded to earlier, for emitting dislocations into a nano-sized grain involves the emission of partial, or perfect, dislocations from sources of stress concentration at grain boundaries. These sites, for example, could include grain boundaries that slide. To explore such a possibility, we examine Fig. 7 which envisages the sliding of a grain facet that, in turn, acts like a small crack. We note, however, that the sliding envisioned here does not constitute gross grain boundary sliding and does not itself produce finite deformation and does not accordingly set limits to strength.

Our procedure is to use the analysis of Rice [45] to explore the critical conditions for the emission of a partial that sets limits to strength. We use the symbol d to represent the length of a *grain boundary facet* that is clearly less than the grain diameter as usually defined. For simple hexagonal grains, this means that the full grain diameter, $\bar{d}$, is twice d, a fact that has significance with respect to our later findings.

Fig. 8 illustrates the basic process whereby a partial dislocation is emitted at the crack tip, with the possibility of the trailing partial dislocation being emitted at higher levels of stress intensity. Note the geometry whereby the angle made by the leading partial Burgers vector is ϕ_1 to the crack tip normal.

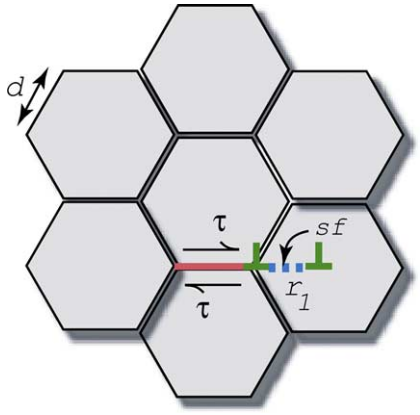

Fig. 7. A model for SF emission from a grain boundary that acts in a crack-like manner. This has the effect of producing a crack with the size of a typical grain facet.

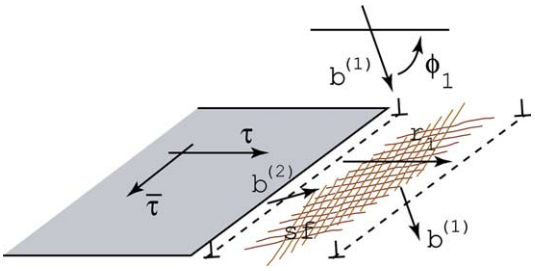

Fig. 8. A model for partial dislocation emission from a grain boundary that acts in a crack-like manner. The crack is loaded via an in-plane mode II applied stress, τ, and an anti-plane mode III shear stress, $\bar{\tau}$.

The lead partial dislocation, after being emitted, travels a distance r_1 into the interior of the grain at initiation, and further into the grain at higher levels of applied load. The effective stress intensities acting on the leading and trailing partial are defined as:

$$K_1 = K_{\mathrm{II}}\cos\phi_1 + K_{\mathrm{III}}\sin\phi_1, \tag{10a}$$

$$K_2 = K_{\mathrm{II}}\cos\phi_2 + K_{\mathrm{III}}\sin\phi_2, \tag{10b}$$

where ϕ_2 is a similarly defined angle as ϕ_1 for the trailing partial. The first partial dislocation is emitted when [45]

$$K_1 \to K_{1\mathrm{crit}} = \sqrt{\frac{2G}{1-\nu}\left[\cos^2\phi_1 + (1-\nu)\sin^2\phi_1\right]\gamma_{\mathrm{us}}}, \tag{11}$$

where γ_{us} is the unstable stacking energy defined in [45] (see later discussion surrounding Fig. 9). At this level of K_1, and then at higher levels, the emitted partial dislocation travels a distance

$$\frac{r_1}{b^{(1)}} = \frac{(K_{1\mathrm{crit}}/K_1)^2}{4\pi(1-\nu)}\,\frac{\cos^2\phi_1 + (1-\nu)\sin^2\phi_1}{\left[1-\sqrt{1-(\gamma_{\mathrm{sf}}/\gamma_{\mathrm{us}})(K_{1\mathrm{crit}}/K_1)^2}\right]^2}\,\frac{Gb^{(1)}}{\gamma_{\mathrm{us}}}. \tag{12}$$

To gain an understanding of the numerology here, let $\phi_1 = 0$. This simplifies the geometry and subsequent determination of the viability of the model vis-à-vis experimental data, such as it exists. If $\phi_1 = 0$, the condition for nucleation of the lead partial dislocation becomes

$$K_{1\mathrm{crit}} = \sqrt{\frac{2G\gamma_{\mathrm{us}}}{1-\nu}} = G\sqrt{\frac{2b^{(1)}}{1-\nu}\Gamma_{1\mathrm{us}}}, \tag{13}$$

where we define a *reduced unstable stacking energy* as

$$\Gamma_{1\mathrm{us}} \equiv \frac{\gamma_{\mathrm{us}}}{Gb^{(1)}}. \tag{14}$$

With the geometric condition $\phi_1 = 0$ imposed, the distance travelled at initiation becomes

$$\frac{r_1}{b^{(1)}} = \frac{(K_{1\mathrm{crit}}/K_1)^2}{4\pi\Gamma_{1\mathrm{us}}(1-\nu)}\,\frac{1}{\left[1-\sqrt{1-(\gamma_{\mathrm{sf}}/\gamma_{\mathrm{us}})(K_{1\mathrm{crit}}/K_1)^2}\right]^2}. \tag{15}$$

When $K_1 = K_{1\mathrm{crit}}$,

$$\frac{r_1}{b^{(1)}} = \frac{1}{4\pi(1-\nu)\Gamma_{1\mathrm{us}}}\,\frac{1}{\left[1-\sqrt{1-(\gamma_{\mathrm{sf}}/\gamma_{\mathrm{us}})}\right]^2}. \tag{16}$$

It is of interest to immediately examine the numerology of Eq. (16).

For Ni, for example, assume that $\gamma_{\mathrm{sf}}/\gamma_{\mathrm{us}} \approx 0.7$ (see later discussion surrounding Table 4) and $\nu \approx 1/3$. From above

$$\Gamma_{1\mathrm{us}} = \sqrt{3}\Gamma\frac{\gamma_{\mathrm{us}}}{\gamma_{\mathrm{sf}}}, \tag{17}$$

where the factor of $\sqrt{3}$ comes from the fact that $b/b^{(1)} = \sqrt{3}$. Thus if $\Gamma = 1/100$ for Ni, then $\Gamma_{1\mathrm{us}} = 1/40$. This means that at initiation of the first partial, $r_1 \approx 5$ nm. As the function $r_1/b^{(1)}$ is a rapidly increasing function of decreasing $(K_{1\mathrm{crit}}/K_1)^2$, when there is but a 20% increase in K_1 from this critical value, $r_1 \approx 10$ nm, and so on. Thus, for materials with grain sizes below 8 nm or so once a partial initiates it tends to traverse the entire grain diameter.

The stress intensity factor for the mode II crack acting on the lead partial is

$$K_{\mathrm{II}} = \tau\sqrt{\pi\frac{1}{2}d}, \tag{18}$$

which brings to light the expected $d^{-1/2}$ grain size dependence for the required shear stress, τ as defined in Fig. 8. In fact, there results for τ the expression

$$\tau/G = \sqrt{\frac{4\Gamma_{1\mathrm{us}}}{\pi(1-\nu)}}\sqrt{\frac{b^{(1)}}{d}} = \zeta\sqrt{\frac{b^{(1)}}{d}}. \tag{19}$$

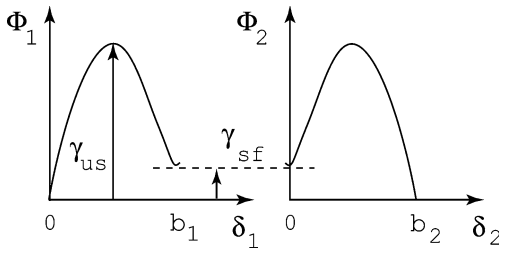

Fig. 9. Energy path experienced by the process of sliding two blocks of crystal, first to create an unstable stacking configuration and then a complete stacking fault. The figure identifies the *unstable stacking energy* and the energy of the end state when a partial dislocation and intrinsic stacking fault has been created.

Table 3
Values for ζ

	Ni	Cu	Al
ζ	0.218	0.251	0.231

Table 3 shows results for the dimensionless quantity $\zeta \equiv (4\Gamma_{1us})/\{\pi(1-\nu)\}^{1/2}$. For Cu, a value of $\Gamma = 1/250$ was used and for Al the stacking fault energy was taken as $\gamma_{sf} = 120$ mJ/m^2. As a further example, for Ni with a grain edge size of 20 nm, and a shear modulus of $G \approx 80$ GPa, the required shear stress becomes, using Eq. (19), $\tau \approx 1540$ MPa, which implies a tensile stress of perhaps $\sigma \approx 2 \times 1540 \approx 3080$ MPa! Results for Cu and Al scale roughly as their respective shear moduli owing to the rough similarity in the value of ζ.

3.1. The trailing partial: perfect dislocation emission

In fcc crystals, the partial dislocation Burgers vectors are inclined in the primary slip plane by a 60° angle. Again setting $\phi_1 = 0$, this results in the criterion for emitting the trailing partial dislocation:

$$\sqrt{3}\left|\frac{K_{III}}{Gb^{(1)}}\right| + \sqrt{\left(\frac{K_{II}}{Gb^{(1)}}\right)^2 - \frac{2\Gamma_{1sf}}{b^{(1)}(1-\nu)}} = \sqrt{\frac{2(4-3\nu)}{b^{(1)}(1-\nu)}}[\Gamma_{1us} - \Gamma_{1sf}], \tag{20}$$

where the reduced stacking fault energy, Γ_{1sf}, is defined as

$$\Gamma_{1sf} \equiv \frac{\gamma_{sf}}{Gb^{(1)}} = \frac{b}{b^{(1)}}\Gamma = \sqrt{3}\Gamma. \tag{21}$$

Here K_{III} is similarly defined, vis-à-vis K_{II}, as

$$K_{III} = \bar{\tau}\sqrt{\pi\frac{1}{2}d}. \tag{22}$$

Note that Eq. (20) is only to be applied after the critical condition for emitting the lead partial dislocation is met so as to ensure that

$$\left(\frac{K_{II}}{Gb^{(1)}}\right)^2 \geqslant \frac{2\Gamma_{1sf}}{b^{(1)}(1-\nu)},$$

since $\gamma_{us} \geqslant \gamma_{sf}$. This assures that the argument of the radical on the left-hand side of Eq. (20) is positive. If $\gamma_{us} \approx \gamma_{sf}$, this criterion leads to the conclusion that the trailing partial is emitted directly after the lead partial dislocation. Metals such as Cu, or Ni, are thereby expected to emit partial dislocations whereas Al may just as readily emit partial, or perfect, dislocations.

At this point, it is worthwhile to view Fig. 9 which illustrates the energy path when two "blocks" of crystal are slipped past each other, first to create an unstable stacking configuration, and then a full stacking fault. The schematic illustrates the energetics involved in the processes of first creating an unstable stacking sequence, leading to the energy level γ_{us}, and the final creation of a stable partial dislocation and an intrinsic stacking fault in the wake of the lead partial dislocation. The intrinsic stacking fault has an energy of γ_{sf}. The trailing partial begins from a system energy level, γ_{sf}, and the system undergoes a similar increase in energy until this second partial dislocation has been fully created. Of course, once formed the "perfect dislocation" will be extended into its two partials that are separated by a distance δ_{eq}, as given by Eq. (4).

Now rewrite Eq. (20), using the result for K_{1crit} from Eq. (13), as

$$\sqrt{3}\left|\frac{K_{III}}{Gb^{(1)}}\right| + \frac{K_{II}}{Gb^{(1)}}\sqrt{1 - \left(\frac{K_{1crit}}{K_{II}}\right)^2\frac{\gamma_{sf}}{\gamma_{us}}} = \sqrt{\frac{2(4-3\nu)}{b^{(1)}(1-\nu)}}\sqrt{\Gamma_{1us}}\sqrt{1-\gamma_{sf}/\gamma_{us}}. \tag{23}$$

At the value of K_{II} where the first partial dislocation is initiated this becomes

$$\sqrt{3}\left|\frac{K_{III}}{Gb^{(1)}}\right| + \frac{K_{1crit}}{Gb^{(1)}}\sqrt{1-\gamma_{sf}/\gamma_{us}} = \sqrt{\frac{2(4-3\nu)}{b^{(1)}(1-\nu)}}\sqrt{\Gamma_{1us}}\sqrt{1-\gamma_{sf}/\gamma_{us}}, \tag{24}$$

which suggests the definition of the quantity β as $\beta \equiv 1 - \gamma_{sf}/\gamma_{us}$. Estimates[3] of this quantity can be obtained from molecular dynamics simulations [43], which are listed in Table 4. The point is, however, that metals such as Ni, Cu, and Al apparently show a wide range of values for the ratio of γ_{sf} to γ_{us} and thus for β. With β close to zero, once the lead partial dislocation has been emitted there is little requirement for an increase in either K_{II} or K_{III} to trigger the emission of the second partial.

Thus, as noted above, the foregoing analysis leads to the expectation that both partial dislocations are emitted in tandem, separated by a spacing set by the intrinsic stacking fault energy and by the action of applied stresses as embodied in the criterion [42] expressed in Eq. (3). If, on the other hand, β is closer to unity we expect that there will often be scenarios where the lead partial dislocations move farther distances out ahead of the boundary, perhaps across the entire grain, before trailing partial dislocations are observed to initiate. There will be a continuous range of scenarios where lead partials will move finite distances and then – with increases in applied stress – be followed by trailing partial dislocations. The relations given above allow for the analysis of these cases, but it is cautioned that the end picture will depend sensitively on the material properties used which, to date, are only very approximately known. Having introduced the parameter β above and taking $\nu \approx 1/3$, Eq. (16) can be rewritten as

$$\frac{r_1}{b^{(1)}} \approx \frac{3}{8\pi\Gamma_{1us}}\frac{1}{[1-\sqrt{\beta}]^2}. \tag{25}$$

[3] We have approximated the values obtained in [43], by using different atomic potentials.

Table 4
Values for β

	Ni	Cu	Al
β	0.30	0.80	0.10

This expression makes clearer the effect of the ratio γ_{sf}/γ_{us} on the distance travelled by the lead partial dislocation at initiation. The range of values for β shown in Table 4 indeed suggests that the effects are significant.

We emphasize that the above development is strictly a two-dimensional analysis and considers no three-dimensional effects such as the existence of what were termed "side segments" in Fig. 5. As such it produces a grain size dependence through the specific picture of the stress concentration arising via a slipping grain boundary facet. A simplified model for the nucleation of a partial dislocation at a crack-like stress concentration at a grain boundary facet is considered below that contains such 3D features. The purpose of this is to explore the possible magnitude of activation volumes that enter the nucleation event as this can provide critical insights into the level of strain rate sensitivity that may be expected.

4. Nucleation of partial dislocations and strain rate sensitivity

There are many vital aspects of the phenomenology of deformation in nanostructured fcc metals that require consideration of mechanistic processes different from those described up to this point. Important among these is the sensitivity of plastic deformation to the loading rate (see Fig. 3). The mechanisms responsible for such strain rate sensitivity remain intriguing. Such large strain rate sensitivity suggests the possibility of a thermally activated process controlling deformation (or initiation) that, in turn, is controlled by an activation volume on the order of, say $3-10b^3$. Thus the foregoing analysis which envisioned a *long and straight* dislocation being emitted should be replaced with one that considers the nucleation of a small loop at a grain boundary facet crack or at a grain boundary triple point.

An analysis of the type done for the emission of a partial, or perfect, dislocation from an assumed *grain boundary facet crack* could be carried out for dislocation nucleation within the locally concentrated stress field of a grain boundary triple point. However, such an analysis would almost immediately raise questions of viability as well. For example, the concentrated field at grain boundary vertices are singular as $\sim 1/r^s$ [46], but with exponents that are directly related to the elastic anisotropy of the crystal. For Al, which is elastically nearly isotropic, such effects would be quite small and presumably no emission would be forecast. For cubic crystals with modest anisotropy, such as many fcc metals, the effects of such stress concentrations are generally not strong [46]. Nonetheless, a careful study is needed especially in light of the fact that molecular dynamic simulations frequently show defects initiated at such sites. Indeed, recent observations of deformation of nanostructured Ni inside the transmission electron microscope [47] reveals nucleation of dislocations at grain boundaries and triple junctions. (Videoimages from this study can be viewed in the website for supplementary material in the electronic archive of [47].) In addition, recent post-indentation studies of polycrystalline Cu with a high density of growth twins also appear to reveal the emission of dislocation loops in deformed twin boundaries [11]. Motivated by these experimental observations, we present next a simplified analysis of a nucleation event to gain insight into the possible magnitude of activation volumes as the grain size is decreased from the microcrystalline to the nanocrystalline regime.

We consider the nucleation of a partial dislocation loop from a stress concentration of the type envisioned above, and as illustrated in Fig. 10. The loop is imagined to be driven out from the crack tip by the concentrated field used in the above analysis. As it happens, however, the segments of the loop are attracted back to the crack tip with an image like force, as described by Asaro and Rice [48]. This is taken into account by choosing for the energy of the expanding, semi-circular, loop the energy per unit length of a full circular loop, viz.

$$\mathscr{L} = Gb_1^2 \frac{2-\nu}{8\pi(1-\nu)} \ln(8r/e^2 r_0), \tag{26}$$

where r_0 is an inner cutoff radius on the order of b_1, and where for convenience of notation we have represented the magnitude of the nucleating, leading, partial dislocation as b_1. Of course, the stress field near the tip of the crack like facet varies as

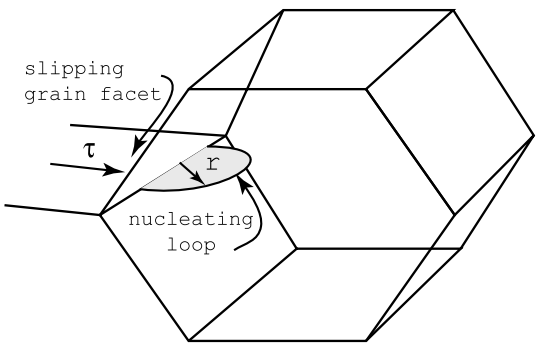

Fig. 10. Nucleation of a partial dislocation loop at the front of a freely slipping grain boundary facet.

$$\sigma_{b_1 m} \approx \frac{K_{\mathrm{II}}}{\sqrt{2\pi r}}, \tag{27}$$

where again $K_{\mathrm{II}} = \tau\sqrt{\pi\tfrac{1}{2}d}$. Each segment of the expanding loop goes through the unstable stacking energy and then leaves an energy wake corresponding to the stacking fault energy. Thus for now, we simply represent the energy per unit area of the loop as γ, where this is to be interpreted vis-à-vis γ_{sf} and γ_{us} once we know the magnitude of r_{c}, the critical radius of the nucleating loop. Now taking in Eq. (26), $8/e^2 \approx 1$, the free energy of the expanding loop is

$$U = \Phi r \ln(r/r_0) - \mathscr{B}(r^{3/2} - r_0^{-3/2}) + \gamma\frac{1}{2}\pi(r^2 - r_0^2), \tag{28}$$

with

$$\Phi = \frac{Gb_1^2(2-\nu)}{8(1-\nu)}, \quad \mathscr{B} = 1.4K_{\mathrm{II}}b_1. \tag{29}$$

Now as $\mathscr{B}$ increases, the system traverses configurations where $r = r(\mathscr{B})$ in which the energy is minimum and then maximum, and where the difference in energy between these extreme states represents an activation energy. To estimate the size of the loop where the process becomes athermal, and is completely mechanically driven, we seek the state where both the conditions:

$$\partial U/\partial r = 0, \tag{30a}$$

$$\partial^2 U/\partial r^2 = 0 \tag{30b}$$

are satisfied. At lower values of $\mathscr{B}$ than this, and thus K_{II} and the applied shear stress, τ, the process is thermally activated. The solution for the critical radius at this athermal state is estimated by noting that $\pi\gamma/\Phi \ll 1$so that, asymptotically, the critical athermal radius is found to be

$$r_{\mathrm{c}} \approx \left(1 + 5\hat{\Gamma}e + \frac{1}{2}[5\hat{\Gamma}e]^2 + \cdots\right)er_0, \tag{31}$$

where $\hat{\Gamma} = \gamma/Gb_1$ is a reduced stacking energy. Some numerical examples follow. If γ is taken as γ_{sf} then, since $1/500 \leqslant \Gamma \leqslant 1/100$ for a wide range of fcc metals, we find that $r_{\mathrm{c}} \approx eb_1$ or $r_{\mathrm{c}} \approx (e/\sqrt{3})b$. This suggests, while momentarily ignoring the effect of $\hat{\Gamma}$, an activation volume on the order of $\upsilon \approx \frac{1}{6}\pi e^2 b^3 \approx \pi b^3$. To assess the effect of stacking fault energy, recall that $\hat{\Gamma} = \sqrt{3}\Gamma$. For Ni, for example, the result in Eq. (31) leads to the estimate $\upsilon \approx 5.3b^3$. At corresponding values of $\mathscr{B}$ less than what exists at this state, the activation area will be larger, but nonetheless such small activation volumes are consistent with the high strain rate sensitivity evident in the data. In particular, activation volumes of the order $5 - 10b^3$ are readily rationalized by the mechanisms we suggest here. To estimate the influence of such a small activation volume we use the definition of experimental activation volume [14]

$$\frac{\partial \ln \dot{\gamma}_{\mathrm{s}}}{\partial \tau} = \frac{\upsilon}{kT}, \tag{32}$$

where the usual definitions of k and T apply and $\dot{\gamma}_{\mathrm{s}}$ is the slip rate. At 300 K, this leads to

$$\delta\tau \approx 70\,\delta \ln \dot{\gamma}_{\mathrm{s}}\ \mathrm{MPa}, \tag{33}$$

or, if τ_1 and τ_2 represent the flow stresses at two levels of strain rate $\dot{\gamma}_{s1}$ and $\dot{\gamma}_{s2}$, respectively, then the difference in flow stress is

$$\tau_1 - \tau_2 \approx 70 \ln(\dot{\gamma}_{s1}/\dot{\gamma}_{s2})\ \mathrm{MPa}. \tag{34}$$

We note that the flow stresses at strain rates of 76 and 1700 s^{-1} are roughly 1700 and 2400 MPa, respectively. Based on the difference between these two strain rates, and using the connection between shear stress and tensile stress $\sigma \approx 2 \times \tau$, Eq. (33) would predict the flow stress at the higher rate to be only 2120 MPa, thus suggesting that the estimate of $\upsilon \approx \pi b^3$ is too large by a factor of 1.6. However, given the approximate nature of our analysis, this level of agreement (compare with the results shown in Fig. 4) is encouraging.

For Ni, if we take the activation volume to be $\upsilon = \pi b^3$, Eq. (34) leads to the result that $\delta\tau \approx 322$ MPa for each factor of 100 increase in strain rate. If again we take the connection between tensile stress and shear stress to be $\sigma \approx 2 \times \tau$, this gives an increment of 644 MPa per factor of 100 increase in strain rate. If instead we had defined the strain rate sensitivity as

$$\frac{1}{m} \equiv \frac{\partial \ln \dot{\gamma}_s}{\partial \ln \tau}, \tag{35}$$

we would have obtained a more consistent measure of rate sensitivity.

The corresponding values of $\mathscr{B}$ are readily calculated and, when done, leads to

$$\frac{\tau}{G} \approx \frac{0.235}{3^{1/4}}\sqrt{\frac{b}{d}} = 0.235\sqrt{\frac{b_1}{d}}. \tag{36}$$

This provides similar conclusions regarding the athermal shear stress required to trigger the injection of a partial dislocation segment. For example, as $b^{(1)} = b_1$ we may compare the value of ζ in Eq. (19) and Table 2 for Ni with this value of 0.235.

Contributions to strain rate sensitivity may also arise from relaxation phenomena occurring at initiation or during dislocation travel [42]. For example, consider Fig. 5 and note the dislocation segments indicated on what is termed the "side boundaries". The energy associated with these segments is reflected in the contribution to the required resolved shear stress by the second term on the right-hand side of Eq. (3). This term is significant and amounts to a contribution to the shear stress of $\delta\tau = \frac{1}{3}\frac{b}{d}G$. For a grain size of 20 nm in Ni, for example, this amounts to an increment in shear stress of $\delta\tau \sim 800$–1000 MPa. Thus there remains the

question of what the actual energetics of such dislocation structure in the side boundaries is, and whether it is affected by strain rate. A complete lack of strain rate sensitivity has been reported [7] for some nanostructured Ni specimens loaded in the quasistatic strain rate range of $10^{-5} - 10^{-2}$, whereas others [28] find a more significant rate dependence. The lack of rate dependence below a certain strain rate range is not consistent with either a truly thermally activated process or with mechanisms such as grain boundary sliding. This again points to the need for more detailed experimental documentation of the full range of strain rate and temperature dependent response in these materials.

Whereas observations of twins and faults have been reported in deformed nanostructured fcc metals, the existing data are somewhat spurious in that statistics for defect densities are lacking as well as correlations of such defect density with imposed inelastic strain. In fact, in many cases of such reports, there is no supporting evidence that the singular observation of a defect such a twin or stacking fault, was even significant with respect to contributing to the measurable inelastic strain. Reliable data of this type are therefore vital for establishing the viability of any proposed mechanism.

5. Emission of deformation twins

Fig. 9 illustrated the energetics of emitting partial dislocations at the tip of a stress concentrator; Fig. 11 goes further to describe both the energetics of emitting partial dislocations and deformation twins (DT) at a crack tip thus defining the *unstable twinning energy*, γ_{ut}. The process of creating a deformation twin has been analyzed by Tadmor and Hai [49] using again Rice's Peierls approach for emitting slip-like defects at a crack tip. The

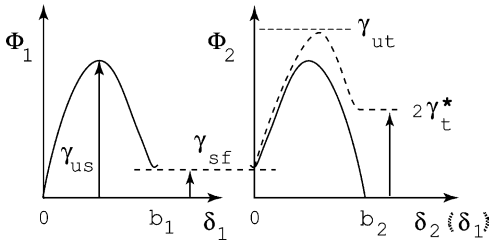

Fig. 11. Energy path for creating a pair of partial dislocations and a deformation twin. The solid line indicates the path for creating the leading partial dislocation, with Burgers vector $\mathbf{b}^{(1)}$ followed by the trailing partial dislocation with Burgers vector $\mathbf{b}^{(2)}$. Between the partial dislocations is an intrinsic stacking fault (SF) with energy γ_{sf}. A deformation twin is created instead by the emission of a second leading partial dislocation on an adjacent slip plane, thereby creating a double twin plane (TP) with a total energy $2\gamma_t^*$; this partial dislocation has again the Burgers vector $\mathbf{b}^{(1)}$.

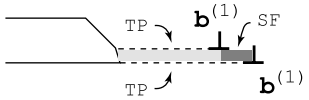

Fig. 12. Emission of a leading partial dislocation followed by the emission of a second leading partial dislocation on an adjacent slip plane, thus creating a deformation twin. The darker shaded region denotes an intrinsic stacking fault and the lighter region a deformation twin. The left side of the figure extends to the boundary from which the fault/twin was emitted.

geometry used by them is the same as used herein. As noted in the caption to Fig. 12, twin creation involves the emission of a second leading partial dislocation on an adjacent slip plane rather than the second partial on the original slip plane. In attempting to compare the tendency for the system to emit either partial dislocation pairs and thus stacking faults, versus twins, a parameter T, termed the *twinning tendency*, is introduced. It is defined as

$$T = \lambda_{\text{crit}} \sqrt{\frac{\gamma_{\text{us}}}{\gamma_{\text{ut}}}}, \tag{37}$$

where γ_{ut} is the *unstable twinning energy* defined in Fig. 11. The reader is referred to the original paper [49] for the details of derivations. The condition $T > 1$ is one that favors twin emission over the emission of the trailing partial dislocation and thus of the emission of faults. Detailed parametric studies of the effects of geometry and material parameters (many of which are only estimated from molecular dynamic simulation) can be found in [49]. Here we simply make contact with our earlier discussion by reducing their analysis vis-à-vis the specific geometric conditions we have used.

The criteria in Eq. (37) pertain to the case where the loading can be expressed by a single parameter and loading direction defined by an angle α, i.e., where the mode II and III stress intensity factors are expressed as

$$K_{\text{II}} = K\cos\alpha, \quad K_{\text{III}} = K\sin\alpha. \tag{38}$$

To explore the possible trends for (or possibility of) twins being emitted along with (or instead of) faults, we examine the case where $\alpha = \phi_1$; we then, as above, look at the case where $\phi_1 = 0$. Recall that the geometric condition $\phi_1 = 0$ defines a state where the leading partial dislocation's Burgers vector is orthogonal to the crack front. Then the parallel case of $\alpha = 0$ means that the direction of shear loading is also orthogonal to the crack front and parallel to the leading Burgers vector. Invoking these geometric assumptions and introducing the parameter (from [49]) that $g \equiv \gamma_{\text{sf}}/\gamma_{\text{us}} = 1 - \beta$, the expression for λ_{crit} becomes simply

$$\lambda_{\text{crit}} = \sqrt{1 + 2\beta}, \tag{39}$$

and twinning tendency parameter, T, becomes

$$T = \sqrt{(1+\beta)\frac{\gamma_{us}}{\gamma_{ut}}}. \tag{40}$$

The analysis assumes elastic isotropy and since the results depend on Poisson's ratio, we have taken $\nu = 0.3$ in all cases. We note, however, that any effects of elastic anisotopy are ignored in [49], a deficiency of little consequence for Al but perhaps of some importance for Cu or Ni. As may be confirmed by examining the various cases explored numerically in [49], the trends expressed by (40) are typical. For example, we use the results of [43] for estimates of γ_{sf}/γ_{us} and γ_{us}/γ_{ut}. They give, respectively, for Al, Cu, and Ni, $\gamma_{us}/\gamma_{ut} = 0.75$, 0.94, 0.786; Tadmor and Hai [49] list for Al and Cu the values $\gamma_{us}/\gamma_{ut} = 0.756$ and 0.894, respectively, which are similar. For λ_{crit} the Van Swygenhoven et al. [43] estimates are $\lambda_{crit} = 1.09$, 1.6, 1.26 for Al, Cu, and Ni, respectively. Thus we obtain for the twinning tendency, $T \approx 0.94$, 1.55, 1.12 for Al, Cu, and Ni, respectively. The trends are, then, to expect that Cu would exhibit the strongest tendency to display twinning modes whereas Al would be less likely to twin.

6. Discussion and conclusions

Our principal objective was to provide a mechanistic rationalization for the consistent observations of high strain rate sensitivity in nanocrystalline fcc metals and alloys. The analysis assumed the existence of a suitable source of stress concentration at a sliding grain boundary facet. In materials with grain sizes below, say, 20 nm or so, this is a reasonable scenario. In materials with much larger grain sizes, this picture becomes less tenable and other sources of stress concentration capable of initiating partial or full dislocations or deformation twins is necessary. Therefore a complete picture that explains the more-or-less continuous decrease in strain rate sensitivity, or alternatively the increase in activation volume, with increasing grain size will require additional analysis that identifies these sites. Scaling that arises from dislocation pictures such as the ones we have analyzed, however, will invariably lead to the trend of increasing activation volume with increasing grain size (or decreasing flow stress). For example, if we consider the homogeneous nucleation of a circular dislocation loop within a grain and use the expression in Eq. (26) for the energy per unit length of a circular dislocation loop we obtain for the total energy

$$\mathscr{E} = Gb^2\frac{2-\nu}{4(1-\nu)}\ln(8r/e^2r_0) - \tau b\pi r^2. \tag{41}$$

Taking again, $8/e^2 \approx 1$ and $\nu \approx 1/3$ and minimizing $\mathscr{E}$ with respect to r we find for the critical radius

$$r_c \approx \frac{5}{16\pi}\left(\frac{\tau}{G}\right)^{-1} b[\ln(r_c/r_0)+1]. \tag{42}$$

To set a stress level, use the criterion for the emission of a full dislocation from a nanocrystalline grain boundary, viz., $\tau/G = b/d$. This yields

$$r_c \approx \frac{5}{16\pi} d(\ln(r_c/r_0)+1). \tag{43}$$

This relation shows that r_c is a monotonically increasing function of grain size d and is in fact more than linearly so. For truly nanocrystalline fcc metals, on the other hand, our mechanistic models do in fact rationalize the very low values of activation volume which are forecast to be in the range $3-10b^3$ consistent with available experimental evidence.

The analysis also points out the importance of considering the complete energy paths involved with generating defects such as partial and full dislocations or twins. In particular, the unstable stacking energy, γ_{us}, introduced by Rice [45] in his analysis of dislocation emission at a crack tip is shown to play an important role in establishing the stress levels required to emit partial dislocations and in assessing the likelihood of the emission of full dislocations and partial dislocations. The importance of this issue is quantified in the present paper through introduction of the parameter, $\beta \equiv 1 - \gamma_{sf}/\gamma_{us}$. The unstable stacking energy is not accessible to direct experimental measurement, but if the trends reported for its ratio with the intrinsic stacking fault energy (which is extracted from molecular dynamics simulations) are used as a guide, the predicted effects are indeed important. For example the term involving β in Eq. (25) which estimates the distance the lead partial dislocation travels after being emitted, i.e., $(1-\sqrt{\beta})^{-2}$, when evaluated for Cu, Ni, and Al would be 90, 5, and 2.17, respectively. This suggests a clear trend for Cu to display extended faults whereas in Al the expectation is for full dislocations to be observed. Trends, at least as seen in molecular dynamics simulations (e.g., see [43]), for full dislocation emission versus fault emission are explained for the most part in the foregoing discussion. Although experimental data at this point are not sufficiently definitive to elucidate the trends with complete clarity, our models clearly indicate that the materials tested to date contain grain size distributions that will lead to various mechanisms occurring concurrently in the same sample.

The experimental observations of rate sensitivity that we have used in our conceptualization and analysis appear to be factually unexceptional. There are, however, difficulties in making direct comparisons of predictions of the various deformation mechanisms with experiment. A major obstacle to unambiguous comparison arises from the fact that all materials tested to date contain a range of grain sizes that, according to our modeling estimates, would indeed span over at least two, and often three, mechanisms.

It must be noted that, in a polycrystal with an average grain size of for example 20 nm, if even 10% of the grains have sizes ranging between 30 and 40 nm that these larger grains will represent essentially 50% of the volume fraction. Distributions such as these are commonly encountered, e.g., see [7]. They have, then, the capacity of dominating the response and leading to flow stress levels far below what may be predicted by models analyzing a strictly 20 nm grain size. If the grain size distribution is truly bi-modal, the smaller grains may act only as non-deforming inclusions. It is, therefore, of great value to obtain data on materials with more uniform grain sizes. The current paucity of such experimental information, and the practical difficulties in producing nanostructured materials with very narrow grain size distributions so that such information can be obtained, also point to a critical need for developing mechanistic models and analyses of the kind presented in this paper.

The mechanistic descriptions presented in this work also point to the manner in which nano-scale growth twins can influence mechanical deformation characteristics, very much like grain boundaries in nanostructured face-centered cubic metals. Such models offer possible means to develop quantitative understanding of the mechanical properties of nanostructured metals for which recent studies have demonstrated appealing opportunities for tailoring strength and hardness by recourse to the controlled introduction of nanoscale twins [11,12,50]. We further note that while the present considerations of both unstable and stable stacking fault energy in the context of GB defect nucleation have drawn a parallel to dislocation emission at the crack tip under mode I [45,52], such mechanistic processes for microcrystalline materials have also been contemplated by recourse to analyses of mixed-mode cracking [53,54].

The expectations for deformation twinning that come out of our analysis are also in good accord with the limited experimental evidence currently available. For example, for Al we would predict that fault emission would be preferred over perfect dislocation emission in pure Al with grain sizes $\bar{d} \leqslant 20$ nm; the twinning tendency parameter suggests that at grain sizes somewhat below this value, deformation twinning becomes possible and eventually preferred. To arrive at this we take for Al $\gamma_{sf} = 142$ mJ/m^2, which gives $\Gamma = 1/77$. Chen et al. [51] indeed report that when the grain size in Al is in the range 10 nm $\leqslant \bar{d} \leqslant 20$ nm mixtures of twins and partial dislocations are observed. Above this range twinning and fault emission are not observed. The relative trends for deformation twinning vs. fault emission vs. perfect dislocation emission noted above for Cu, Ni, Al, etc. are, as expected, in general agreement with known observations.

Acknowledgments

R.J.A. is thankful to the National Science Foundation for support under the NIRT initiative. S.S. acknowledges support of this work by the Defense University Research Initiative on Nano Technology (DURINT) on ''Damage- and Failure-Resistant Nanostructured and Interfacial Materials'' which is funded at the MIT by the Office of Naval Research under Grant No. N00014-01-1-0808.

References

[1] Hall EO. The deformation and ageing of mid steel: III discussion of results. Proc Phys Soc Lond, Sect B 1951;64:747–53.
[2] Petch NJ. The cleavage of polycrystals. J Iron Steel Inst 1953;174:25–8.
[3] Gleiter H. Nanocrystalline materials. Prog Mater Sci 1989;33(4):223–315.
[4] Kumar KS, Van Swygenhoven H, Suresh S. Mechanical behavior of nanocrystalline metals and alloys. Acta Mater 2003;51(19):5743–74.
[5] Lu L, Li SX, Lu K. An abnormal strain rate effect on tensile behavior in nanocrystalline copper. Scripta Mater 2001;45(10):1163–9.
[6] Wang YM, Ma E. Temperature and strain rate effects on the strength and ductility of nanostructured copper. Appl Phys Lett 2003;83(15):3165–7.
[7] Dalla Torre F, Van Swygenhoven H, Victoria M. Nanocrystalline electrodeposited Ni: microstructure and tensile properties. Acta Mater 2002;50(15):3957–70.
[8] Schwaiger R, Moser B, Chollacoop N, Dao M, Suresh S. Some critical experiments on the strain-rate sensitivity of nanocrystalline nickel. Acta Mater 2003;51(17):5159–72.
[9] Wei Q, Cheng S, Ramesh KT, Ma E. Effect of nanocrystalline and ultrafine grain sizes on the strain rate sensitivity and activation volume: fcc versus bcc metals. Mater Sci Eng A 2004;381:71–9.
[10] Wang YM, Ma E. Strain hardening, strain rate sensitivity, and ductility of nanostructured metals. Materials Sci Eng A 2004;375–377:46–52.
[11] Lu L, Schwaiger R, Shan ZW, Dao M, Lu K, Suresh S. Nano-sized twins induce high rate sensitivity of flow stress in pure copper. Acta Mater 2005;53(7):2169–79.
[12] Lu L, Shen Y, Chen X, Lu K. Ultrahigh strength and high electrical conductivity in copper. Science 2004;304:422–6.
[13] Conrad H. In: Zackey VF, editor. High strength materials; 1965.
[14] Krausz AS, Eyring H. Deformation kinetics. New York (NY): Wiley; 1975. p. 117–21.
[15] Sanders PG, Eastman JA, Weertman JR. Elastic and tensile behavior of nanocrystalline copper and palladium. Acta Mater 1997;45(10):4019–25.
[16] Champion Y, Langlois C, Mailly SG, Langlois P, Bonnentien JL, Hytch MJ. Science 2003;300:310.
[17] Legros M, Elliott BR, Rittner MN, Weertman JR, Hemker KJ. Microsample tensile testing of nanocrystalline metals. Philos Mag A 2000;80(4):1017–26.
[18] Iyer RS, Frey CA, Sastry SML, Waller BE, Buhro WE. Plastic deformation of nanoscale Cu and Cu–Co–0.2 wt.%B. Mater Sci Eng 1999;A264:210–4.
[19] Gertsman VY, Hoffman M, Gleiter H, Birringer R. The study of grain-size dependence of yield stress of copper for a wide grain-size range. Acta Metall Mater 1994;42:3539.

[20] Wang YM, Ma E, Chen MW. Enhanced tensile ductility and toughness in nanostructured Cu. Appl Phys Lett 2002;80:2395–7.
[21] Youssef KM, Scattergood RO, Murty KL, Koch CC. Ultratough nanocrystalline copper with a narrow grain size distribution. Appl Phys Lett 2004;85:929–31.
[22] Valiev RZ, Alexandrov IV, Zhu YT, Lowe TLC. Paradox of strength and ductility in metals processed by severe platic deformation. J Mater Res 2002;17:5–8.
[23] Hughes GD, Smith SD, Pande CS, Johnson HR, Armstrong RW. Hall–Petch strengthening for the microhardness of 12 nanometer grain diameter electrodeposited nickel. Scripta Metall 1986;20(1):93–7.
[24] Elsherik AM, Erb U, Palumbo G, Aust KT. Deviations from Hall–Petch behavior in as-prepared nanocrystalline nickel. Scripta Metall Mater 1992;27(9):1185–8.
[25] Mitra R, Hoffman RA, Madan A, Weertman JR. Effect of process variables on the structure, residual stress, and hardness of sputtered nanocrystalline nickel films. J Mater Res 2001;16(4):1010–27.
[26] Schuh CA, Nieh TG, Yamasaki T. Hall–Petch breakdown manifested in abrasive wear resistance of nanocrystalline nickel. Scripta Mater 2002;46(10):735–40.
[27] Ebrahimi F, Bourne GR, Kelly MS, Matthews TE. Mechanical properties of nanocrystalline nickel produced by electrodeposition. Nanostruct Mater 1999;11(3):343–50.
[28] Bailey R, Asaro RJ. University of California at San Diego, La Jolla, CA; 2004 [unpublished results].
[29] Schiotz J, Di Tolla FD, Jacobsen KW. Softening of nanocrystalline metals at very small grain sizes. Nature 1998;391(6667):561–3.
[30] Van Swygenhoven H, Caro A, Farkas D. Grain boundary structure and its influence on plastic deformation of polycrystalline FCC metals at the nanoscale: a molecular dynamics study. Scripta Mater 2001;44:1513–6.
[31] Yamakov V, Wolf D, Phillpt SR, Gleiter H. Grain boundary diffusion creep in nanocrystalline palladium by molecular dynamics simulation. Acta Mater 2002;50:61–73.
[32] Chokshi AH, Rosen A, Karch J, Gleiter H. On the validity of the Hall–Petch relationship in nanocrystalline materials. Scripta Metall 1989;23:1679–84.
[33] Van Vliet K, Tsikata J, Suresh S. Model experiments for direct visualization of grain boundary deformation in nanostructured metals. Appl Phys Lett 2003;83(7):1441–3.
[34] Knapp JA, Follstaedt DM. Hall–Petch relationship in pulsed-laser deposited nickel films. J Mater Res 2004;19(1):218–27.
[35] Follansbee PS, Kocks UF. A constitutive description of the deformation of copper based on the use of the mechanical threshold stress as an internal state variable. Acta Metall 1988;36:81–93.
[36] Carrekar RP, Hibbard WR. Tensile deformation of high-purity copper as a function of temperature, strain rate, and grain size. Acta Metall 1953;1:64–663.
[37] Follansbee PS, Regazzoni G, Kocks UF. Mechanical properties of materials at high strain rates of strain. In: Inst Phys Conf Ser 70, The Institute of Physics; 1984. p. 71.
[38] Conrad H, Narayan J. On the grain size softening in nanocrystalline materials. Scripta Mater 2000;42(11):1025–30.
[39] Conrad H. Grain size dependence of the plastic deformation kinetics in Cu. Mater Sci Eng A 2003;341(1–2):216–28.
[40] Ma E. Watching the nanograins roll. Science 2004; 305(5684):623–4.
[41] Gray GT et al. Influence of strain rate and temperature on the mechanical response of ultrafine-grained Cu, Ni, and Al–4Cu–0.5Zr. Nanostruct Mater 1997;9(1–8):477–80.
[42] Asaro RJ, Krysl P, Kad B. Deformation mechanism transitions in nanoscale fcc metals. Philos Mag Lett 2003;83(12):733–43.
[43] Van Swygenhoven H, Derlet PM, Froseth AG. Stacking fault energies and slip in nanocrystalline metals. Nat Mater 2004;3(6):399–403.
[44] Barnett DM, Asaro RJ. The fracture mechanics of slit-like cracks in anisotropic elastic media. J Mech Phys Solids 1972;20:353–60.
[45] Rice JR. Dislocation nucleation from a crack tip – an analysis based on the Peierls concept. J Mech Phys Solids 1992;40(2):239–71.
[46] Ghahremani F, Hutchinson JW. Three-dimensional effects in microcrack nucleation in brittle polycrystals. J Am Ceram Soc 1990;73:1548–54.
[47] Kumar KS, Suresh S, Chisholm MF, Horton JA, Wang P. Deformation of electrodeposited nanocrystalline nickel. Acta Mater 2003;51(2):387–405.
[48] Asaro RJ, Rice JR. Strain localization in ductile single crystals. J Mech Phys Solids 1977;25(2):309–38.
[49] Tadmor EB, Hai S. A Peierls criterion for the onset of deformation twinning at a crack tip. J Mech Phys Solids 2003;53(3):765–93.
[50] Wu BYC, Ferreira PJ, Schuh C. Nanostructured Ni–Co alloys with tailorable grain size and twin density. 2004 [submitted].
[51] Chen M, Ma E, Hemker KJ, Sheng H, Wang Y, Cheng X. Deformation twinning in nanocrystalline aluminum. Science 2003;300:1275–7.
[52] Rice JR, Beltz GE, Sun Y. Peierls framework for dislocation nucleation from a crack tip. In: Argon AS, editor. Topics in fracture and fatigue. New York (NY): Springer-Verlag; 1992. p. 1–58.
[53] Xu G, Argon AS, Ortiz M. Nucleation of dislocations from crack tips under mixed modes of loading: implications for brittle against ductile behaviour of crystals. Philos Mag A 1995;72(2): 415–51.
[54] Xu G, Argon AS, Ortiz M. Critical configurations for dislocation nucleation from crack tips. Philos Mag A 1997;75(2):341–67.